RNA methylation-mediated LINC01559 suppresses colorectal cancer progression by regulating the miR-106b-5p/PTEN axis

Ke Shi
Zhengzhou University First Affiliated Hospital
Shuaixi Yang
Zhengzhou University First Affiliated Hospital
Quanbo Zhou
Zhengzhou University First Affiliated Hospital
Chen Chen
Zhengzhou University
Bo Shao
Zhengzhou University First Affiliated Hospital
Yaxin Guo
Zhengzhou University
Xiaoke Wu
Zhengzhou University First Affiliated Hospital
Luyang Zhao
Zhengzhou University
Xiuxiu Yang
Zhengzhou University
Qiuge Zhang
Zhengzhou University First Affiliated Hospital
Guixian Wang
Zhengzhou University First Affiliated Hospital
Weitang Yuan
Zhengzhou University First Affiliated Hospital
Jinbo Liu
Zhengzhou University First Affiliated Hospital
Zhenqiang Sun (fccsunzq@zzu.edu.cn)
Zhengzhou University First Affiliated Hospital

Research

Keywords: LINC01559, PTEN, METTL3, colorectal cancer

Posted Date: March 1st, 2021

DOI: https://doi.org/10.21203/rs.3.rs-261378/v1

Abstract

Background

Long noncoding RNAs (lncRNAs) regulate multiple biological effects in cancers. Recently, RNA methylation has been found to modify not only coding RNAs but also some noncoding RNAs. How RNA methylation affects lncRNAs to affect colorectal cancer (CRC) progression remains elusive.

Methods

RNA-sequencing of cancer and normal tissues was analysed. LINC01559 in CRC was selected and verified by western blot (WB), quantitative real-time PCR (qRT-PCR) and in situ hybridization (ISH). Functional experiments in vitro and in vivo were used to explore the biological functions of LINC01559 in CRC. The LINC01559/miR-106-5p/PTEN axis was explored at different levels of analysis, including fluorescence in situ hybridization (FISH), luciferase assays, and rescue experiments. RIP-sequencing, m6A RNA immunoprecipitation (MeRIP) assays and bioinformatic analysis were conducted to determine the upstream mechanism of LINC01559.

Results

LINC01559, identified by RNA-sequencing analysis, was downregulated in CRC tissues and cell lines compared with normal controls. Lower expression of LINC01559 in CRC patients predicted a poor prognosis. In addition, PTEN was found to be positively correlated with LINC01559, and bioinformatic analysis and in vitro experiments indicated that miR-106b-5p could be the link between LINC01559 and PTEN. Then, downregulated LINC01559 restored the malignant phenotype of CRC cells in vivo and in vitro, while cotransfection of si-LINC01559 and miR-106b-5p inhibitor neutralized this effect. Notably, METTL3 was found to be highly expressed in CRC, and the downregulation of METTL3 could inhibit the migration and invasion of CRC cells. Mechanistically, we found abundant m6A modification sites on LINC01559. Then, we uncovered these sites as potential targets of METTL3 through experiments *in vivo*.

Conclusion

The results revealed a negative functional regulation of LINC01559/miR-106b-5p/PTEN axis in CRC progression, and explored a new mechanism of METTL3-mediated m6A modification on LINC01559 formation. These results elucidate a novel potential therapeutic target for CRC treatment.

Trial registration

The human cancer tissues used in this study were approved by Ethnics Committee of The First Affiliated Hospital of Zhengzhou University in December 19, 2019, and the TRN is 2019-KW-423.

Background

Colorectal cancer (CRC) (CRC) third in terms of incidence and is a significant cause of morbidity and mortality worldwide [1–3]. Over 1.8 million new CRC cases and 881,000 deaths occurred in 2018, accounting for approximately 1 in 10 cancer cases and deaths [1]. Although the overall survival (OS) of CRC patients has improved with the development of medical technology, the outcome of advanced-stage colorectal cancer patients remains poor [3]. Therefore, more effective and efficient biomarkers and molecular mechanisms need to be investigated in both the diagnosis and the treatment of CRC.

Long noncoding RNAs (lncRNAs) are a newly emerged class of noncoding RNAs containing more than 200 nucleotides that are widely transcribed in the genome [4, 5]. Due to the diverse cellular functions of lncRNAs, they play essential roles in almost every cellular process, including proliferation, differentiation and apoptosis [6, 7]. Furthermore, mechanistic studies have shown that lncRNAs can affect chromatin structure and RNA interactions, such as their function as a microRNA (miRNAs) sponge, in which lncRNAs can interact with miRNAs through their seed sequences to reduce the miRNA regulatory effect on target mRNAs.

In recent years, the use of lncRNA high-throughput sequencing for the diagnosis of Mendelian or rare genetic disorders has become routine clinical practice [2]. LncRNA-sequencing could reveal the dynamic process of gene transcription, which varies according to tissue type, cellular conditions, and environmental factors and may affect regulatory events such as splicing and the expression of genes or their isoforms [8]. LncRNA high-throughput sequencing with cluster analysis of differentially expressed lncRNAs could identify the expression patterns of different genes under different biological or experimental conditions and aggregate lncRNAs with the same or similar expression patterns [9]. Information from chromosome distribution analysis could further reveal important relationships with gene functions [10]. Therefore, the importance of lncRNA-sequencing as a clinical diagnostic tool has increased. Through analyses of the differential expression of lncRNAs and their positions on chromosomes, it was revealed that LINC01559 was expressed at low levels in CRC tissues and located in chromosome mapping to 12p12-12p13.1, which is always absent from mutations in human tumors[11]. However, the potential biological functions, characteristics and mechanisms of LINC01559 in CRC progression have not been elucidated in the pioneering studies.

N6-methyladenosine (m6A) RNA methylation is one of the most ubiquitous internal modifications on eukaryotic messenger RNAs (mRNAs), accounting for approximately 50% of total methylated ribonucleotides and 0.1–0.4% of all adenosines in total cellular RNAs [12]. Previous research has shown that over 300 noncoding RNAs in humans and mice are found through m6A-specific immunoprecipitation (MeRIP-Seq) [13]. Moreover, m6A modification in noncoding RNAs could play a critical role in virtually all major normal bioprocesses, including stem cell self-renewal and differentiation, tissue development, heat shock or DNA damage response, maternal-to-zygotic transition, primary microRNA processing, and RNA–protein interactions [12]. As lncRNAs are transcribed and modified similarly to messenger RNA (though typically with many more m6A sites), m6A RNA methylation may more actively regulate lncRNAs than what we had known, through a mechanism similar to mRNA.

Mechanistically, The dynamic and reversible N6-methyladenosine (m6A) RNA modification preferentially occurs in the consensus motif “RRm6ACH” (R = G or A; H = A, C or U) and is mediated by m6A WERs (“writers”, “erasers” and “readers”), including the m6A “writer” methyltransferase METTL3 [14, 15]. A growing number of studies have confirmed the functions of m6A in a variety of malignancies. Nevertheless, the definite role of m6A in CRC remains unclear, and the dysregulation of METTL3-mediated m6A modification in the progression of CRC needs to be further explored.

In this study, the RNA sequencing results of CRC and paired normal tissues showed that LINC01559 was expressed at low levels in CRC tissues compared with paired normal tissues. QRT-PCR analyses of CRC tissues and cell lines also proved the downregulation of LINC01559 in CRC, and low LINC01559 expression in CRC patients predicted poor survival. Furthermore, we investigated the downstream mechanism of LINC01559. Combined with the results of rescue experiments, LINC01559 could regulate the miR-106b-5p/PTEN axis to influence the biological functions of CRC cells. The former mechanistic investigations of LINC01559 showed that METTL3 could methylate the m6A sites of LINC01559 to affect the functions of CRC cells.

Methods

Clinical samples

Fresh colorectal cancer tissues and paired adjacent normal specimens were collected by surgical resection from the First Affiliated Hospital of Zhengzhou University. The patients with colorectal cancer had received neither chemotherapy nor radiotherapy prior to resection. Pathological diagnostics for colorectal cancer were determined by three pathologists. The tumor stage was determined according to the eighth edition of the International Union Against Cancer (UICC)/American Joint Committee on Cancer (AJCC) TNM classification [16]. The clinical characteristics of the 30 CRC patients are presented in Table 1.

Prior to the use of these clinical materials, written consent was obtained from all patients, and approval was obtained from the First Affiliated Hospital of Zhengzhou University Ethical Review Committees. None of the patients received any preoperative chemotherapy or radiotherapy.

Table 1
Univariate analyses of relationship between LINC01559 and clinicopathological parameters in patients with CRC.

	n	LINC01559		χ^2	*P*
		Low	High		
Age				0.141	0.707
< 60	19	11	8		
≥ 60	22	14	8		
Gender				2.169	0.141
Male	16	12	4		
Female	25	13	12		
Tumor size (cm)				0.137	0.412
< 5	25	16	9		
≥ 5	7	5	2		
Tumor location				0.570	0.450
Colon	10	7	3		
Rectum	30	17	13		
Histological differentiation				2.575	0.109
Well/ middle	15	7	8		
Poorly/ undifferentiated	22	16	6		
TNM stage				9.471	0.002
I/II/III	20	17	3		
IV	21	8	13		
Lymph node metastasis				5.184	0.023
Yes	25	19	6		
No	16	6	9		
Distant metastasis				6.740	0.009
Yes	18	15	3		
No	23	10	13		
Perineural invasion				0.577	0.448

	n	LINC01559		χ^2	*P*
Yes	10	5	5		
No	25	16	9		
Vascular invasion				0.162	0.685
Yes	14	9	5		
No	26	15	11		

Bioinformatic analysis

In our research, KEGG analysis provided information about the signalling pathways in CRC (Additional file 1: Figure S1) [17, 18]. The data from GEPIA (http://gepia.cancer-pku.cn/index.html) were utilized to analyse the correlation between PTEN and key molecules in different signalling pathways (Additional file 2: Figure S2) [19]. The selection of potential miRNAs was performed by DIANA tools-Tarbase v8 (http://www.microrna.gr/tarbase) and DIANA tools-LncBase Predicted v2 (www.microrna.gr/LncBase) [20], and then a Venn diagram (http://www.cmbi.ru.nl/cdd/biovenn/) was utilized to intersect the two datasets [21] (Additional file 3: Table S1). Furthermore, we obtained GXE49246, GSE115513, GSE41655, GSE108153, GSE110402 and GSE56350 from GEO (http://www.ncbi.nlm.nih.gov/geo/) [22]. Starbase3.0 (http://starbase.sysu.edu.cn/) was used to analyse binding site sequences of miR-106b-5p on LINC01559 and miR-106b-5p on PTEN [23]. Then, the potential methylated sites of LINC01559 and miR-106b-5p were explored by RMBase v2.0 (http://rna.sysu.edu.cn/rmbase/) and SRAMP (http://www.cuilab.cn/sramp) [24] (Additional file 4: Table S2, Additional file 6: Figure S3, Additional file 12: File S1) .

In situ hybridization (ISH), imaging and scoring

After the tissue was dewaxed, it was incubated with the pre-hybridization solution and subsequently hybridized with the LINC01559 and miR-106b-5p probes. Then, visualization of the staining was performed using DAB. CRC cells were fixed by 4% paraformaldehyde in PBS for 20 min at room temperature. According to the manufacturer's instructions, the LINC01559 and miR-106b-5p probes were used with a Fluorescent In Situ Hybridization Kit (RiboBio, Guangzhou, China) in HCT116 and SW480 cells. Finally, the image was obtained using confocal laser scanning microscopy (ZEISS, Jena, Germany). The signal intensities of LINC01559 and miR-106b-5p expression were quantified by using the intensity measurement tools of the Image-Pro Plus software package (Media Cybernetics, Houston, America). For quantification of ISH staining, samples were scored in a blind manner, and a staining H-score was calculated for each section, where H-score = Σ (% of cells with 4×4) + (% of cells with 3×3) + (% of cells with 2×2) + (% of cells with 1×1), in which 0 = no staining, 1 = weak, 2 = moderate, 3 = intense and 4 = very intense staining [25].

Tumor xenografts in animals and functional assaysin vivo

A total of 1×10^6 HCT116-RNAa-LINC01559, HCT116-RNAi-LINC01559, or control SW480 cells were injected subcutaneously into the left and right flanks of 4- to 6-week-old BALB/c-nu/nu athymic nude mice (n = 5 per group) acquired from Vital River Laboratory (Beijing, China). tumor growth was visualized and imaged using a whole-body GFP imaging system (Lighttools, Encinitas, CA). tumor size was measured by a slide calliper, and tumor volume was calculated as follows: volume = (D×d2)/2, where D was the longest diameter and d was the shortest diameter. For testing *in vivo* proliferation, the subcutaneous tumors were diced into 1 mm^3 cubes and implanted into the mesentery at the caecum terminus of the nude mice. Animals were kept until the end of the experiment (20 days). The organs were fixed with 10% neutral buffered formalin and paraffin-embedded. Subsequently, consecutive tissue sections were made for each block and stained with haematoxylin-eosin (H&E) and immunohistochemistry (IHC) staining to observe the tumors in organs under a microscope. All specimens were examined under a light microscope (Nikon, Japan). Villus height and crypt depth were measured using an image analysis system.

The experiments were performed according to institutional guidelines and approved by the Institutional Animal Care and Use Committee of Southern Medical University.

RNA fluorescence in-situ hybridization (FISH)

RNA FISH assays were performed to observe LINC01559 location. SW480, lovo and HCT116 cells were fixed by 4% formaldehyde for 10 min at room temperature and then permeabilized using 0.5% Triton X-100 for 30 min. Afterwards, the cells were washed 3 × for 5 min in PBS and then hybridized with cDNA probe labelled with fluorochrome Cy3 (green) (Fig. 5e, Additional file 8: Figure S4).

Luciferase reporter assay

Wild type LINC01559 with potential miR-106b-5p binding sites and a mutant of each site were generated and fused to the luciferase reporter vector psiCHECK-2 (Promega, Madison, WI, USA). The full-length wild-type (WT) 3’ untranslated region (UTR) containing the predicted miR-106b-5p targeting site and the mutant-type (MT) 3’-UTR with a mutated miR-106b-5p binding site were amplified and cloned into the psiCHECK-2 vector. SW480 cells were placed on a 24-well plate and grown to 80% confluence. Cells were then cotransfected with luciferase plasmids and miR-106b-5p or control miRNA. After 48 h of transfection, firefly and Renilla luciferase activities were measured with a Dual-Luciferase Reporter Assay System (Promega). The same method was manipulated to investigate the miR-106b-5p target sites in PTEN.

RNA-immunoprecipitation assay (RIP) and RIP-sequencing (RIP-seq)

A Magna RIP RNA-Binding Protein Immunoprecipitation Kit (Millipore, USA) was used according to the manufacturer’s instructions. Briefly, cells were collected and lysed by RIP lysis buffer. Then, magnetic beads coated with 5 μg of specific antibodies against mouse immunoglobulin G (17–700, Millipore) or

METTL3 (Proteintech, Wuhan, China) were incubated with prepared cell lysates with rotation overnight at 4°C. Then, the complexes were washed 6 times, and the precipitate was digested with Proteinase K buffer. Then, RNA was extracted by phenol-chloroform RNA extraction methods. Finally, library preparation was performed for RNA samples using the Illumina TruSeq Stranded mRNA Sample Prep Kit. No mRNA or rRNA depletion steps were performed. Libraries were sequenced by 50 bp paired-end sequencing.

M6A RNA immunoprecipitation (MeRIP) assay

MeRIP was performed using the Magna MeRIP m6A Kit (Qiagen, Germany) according to the manufacturer's instructions. Briefly, 3 μg of anti-m6A antibody (Synaptic Systems, Goettingen, Germany) was conjugated to protein A/G magnetic beads overnight at 4°C. Then, the antibody-conjugated beads were incubated with the antibody in IP buffer with RNase inhibitor and protease inhibitor. The interacting RNAs were isolated and detected by qRT-PCR.

Statistics

All statistical analyses were carried out with SPSS version 18.0 (MT, USA) and GraphPad Prism 5.0 software (CA, USA). Data are expressed as the mean ± SEM. Two groups pairs were compared by Student's t-test. Pearson's coefficient was used to assess the correlations between variables. Survival data were obtained by the Kaplan–Meier method, with significance assessed by the log-rank test. The associations of LINC01559 expression and clinicopathologic variables were assessed by the Chi-square test or Fisher's exact test. Median LINC01559 expression levels were the cutoff points for determining high and low expression. $P < 0.05$ was considered statistically significant. Other methods are summarized in Supplemental information.

Results

1. LINC01559 is expressed at low levels in CRC, and the downregulation of LINC01559 is associated with poor prognosis.

Genomic copy number aberrations are believed to be an important driver of tumorigenesis [13, 26]. It has also been reported that the 12p12-12p13.1 region to which p27Kipl maps is of interest in relation to cancer, including CRC [11, 27]. Thus, we investigated the dynamics of lncRNA alterations through high-throughput lncRNA sequencing of 4 CRC tissue samples and 3 normal intestinal mucosa samples. Within these genomic loci, LINC01559 met the four following requirements: step 1: lncRNAs showing statistically significant dysregulation by p value and q value < 0.05; step 2: lncRNAs downregulated in tumor samples compared with normal samples; step 3: lncRNAs with expression > 0 in 7 samples; step 4: the host genes of lncRNAs located in the chromosomal region 12p12-12p13.1 and included in the Gene database (Fig. 1A, $P<0.05$). The clustered heatmap shows that 164 lncRNAs were identified after the selection at step 4 (Fig. 1B).

Next, six pairs of fresh cancer tissues and adjacent normal tissues from CRC patients were collected. The adjacent tissues were normal intestinal mucosa that were more than 5 cm away from the tumor sites.

The lncRNA expression profiles, determined by high-throughput sequencing, showed that several lncRNAs were downregulated in CRC tissues. LINC01559 was expressed at lower levels in CRC tissues than in paired normal tissues (Fig. 1C, $P<0.01$). To verify the reliability of the high-throughput RNA sequencing data, the RNA expression level of LINC01559 was detected by qRT-PCR in 41 pairs of tissues (Fig. 1D, $P<0.0001$) and 4 different cell lines, FHC, HCT116, SW480 and H29 (Fig. 1E). The results revealed that LINC01559 was downregulated in CRC tissues and CRC cell lines compared to the normal group. To further characterize the association between LINC01559 expression and the outcome of CRC, the patients were stratified according to the expression level of LINC01559. The Kaplan-Meier curves showed that a low expression level of LINC01559 was associated with shorter disease-free survival in CRC patients (Fig. 1F). Then, we performed ISH staining to analyse LINC01559 expression and distribution in 30 pairs of CRC tissues and adjacent normal tissues from CRC patients with different TNM stages (Fig. 1G). Combined with analyses of the H-score, the results demonstrated that LINC01559 expression was lower in CRC tissues with different degrees of malignancy than in normal tissues (Fig. 1H).

A total of 30 patients, 18 males and 12 females, were examined. Their clinicopathological features are shown in Table 1. We selected the quartile expression of LINC01559 of 41 patients to be the ideal cutoff value. Then, the CRC patients were divided into a high-expression level group (25 cases) and a low-expression level group (16 cases). Chi-square tests showed that the different expression levels of LINC01559 were independently associated with TNM stage ($P<0.05$), lymphatic metastasis ($P<0.05$) and distant metastasis ($P<0.01$). Age, gender, tumor location, degree of differentiation, neural infiltration and vascular invasion were not significantly different between the LINC01559 expression groups ($P>0.05$). In conclusion, LINC01559 is expressed at low levels in CRC, and downregulated LINC01559 expression leads to poor prognosis, which indicates that LINC01559 is a tumor suppressor marker in CRC.

2. Downregulated LINC01559 enhances CRC cell proliferation and metastasis *in vitro*.

A qRT-PCR assay was utilized to estimate LINC01559 expression in HCT116 and SW480 cells. Then, we chose si-LINC01559-3 as a representative siRNA specific to LINC01559 on account of its strong knockdown efficiency (Additional file 7: Figure S5). To assess the functions of LINC01559 in CRC cell lines, tumor cell proliferation was evaluated by CCK-8 and EdU assays. The results showed that silencing LINC01559 expression in HCT116 and SW480 cells considerably increased tumor proliferation (Fig. 2A, 2B). Furthermore, we used a wound healing assay to investigate whether LINC01559 was involved in the metastasis of tumor cells. The results showed that silencing LINC01559 expression in HCT116 and SW480 cells considerably induced their migration. Wound healing and transwell assays revealed that, unlike transfection with the negative control sequence, siRNA-mediated knockdown of LINC01559 increased the metastasis of HCT116 and SW480 cells (Fig. 2C, 2D). Then, a tube formation assay was utilized to estimate the vascular formation ability of tumor cells. The results revealed that transfection with si-LINC01559-3 markedly induced vascularization in HCT116 and SW480 cells (Fig. 2E). To investigate the potential mechanism of LINC01559, the qRT-PCR assay demonstrated that silencing LINC01559 obviously repressed the expression of BCL-2 ($P<0.05$) in both HCT116 cells and SW480 cells and E-cadherin in SW480 cells ($P<0.01$). Silencing LINC01559 upregulated the expression of MMP2

(P<0.05) and MMP9 (P<0.05) in the two cell lines, BAX (P <0.05) in HCT116 cells, and N-cadherin (P<0.01) and ZEB1 (P <0.05) in SW480 cells (Fig. 2F). Overall, silencing LINC01559 restricted this inhibitory effect on CRC cell proliferation and metastasis *in vitro*.

3. Downregulated LINC01559 promotes CRC progression *in vivo*.

To test the hypothesis that LINC01559 inhibits CRC progression, we transduced empty retroviral expression vectors and retroviral expression vectors with the anti-LINC01559 sequence into HCT116 cells. For comparison, the LINC01559 expression difference between the anti-LINC01559 negative control (anti-LINC01559 Ctl) and anti-LINC01559 in HCT116 cells was statistically significant (P<0.05) (Fig. 3A). Then, the two groups of HCT116 cells were inoculated into nu athymic nude mice. After inoculation, the nude mice were randomly assigned into two groups of five mice each: anti-LINC01559 negative control group (LN, treated with HCT116 cells transfected with empty vector) and anti-LINC01559 (LA, treated with HCT116 cells transfected with LINC01559 siRNA vector). Then, we observed tumor growth for 21 days and measured tumor volume and weight (Fig. 3B). The results showed that the tumor volume (P<0.01) and tumor weight (P<0.01) in the LA group were significantly higher than those in the LN group at the end of observation (Fig. 3C, 3D, 3E). The WB assays demonstrated that the protein expression of ZO1 was also significantly downregulated in the LA group, while the protein expression of p-AKT was the opposite in the LA group (Fig. 3F). Furthermore, H&E staining was utilized to observe angiogenesis in the two groups. The results revealed that silencing LINC01559 considerably increased tumor vascularization (Fig. 3G). IHC staining demonstrated that the protein expression levels of PTEN, p-AKT, N-cadherin and VIM were significantly increased in the LA group, while the results for E-cadherin and ZO1 were the opposite (Fig. 3H, Fig.4G). In summary, downregulated LINC01559 could enhance CRC cell progression *in vivo* by regulating CRC proliferation, angiogenesis and functional protein expression.

4. PTEN is associated with LINC01559 and is expressed at low levels in CRC.

PTEN is a tumor suppressor gene, and a downregulated PTEN expression status is associated with poor survival in CRC, which has been well characterized [28, 29]. Considering that our noncoding RNA of interest, LINC01559, acts as a suppressor in CRC, we hypothesized that LINC01559 might influence the expression of PTEN. Next, we collected the key signalling pathways of CRC and analyzed the correlation between PTEN and key molecules in these signalling pathways (Additional file 5: Table S3, Additional file 9: Figure S5). The results showed that PTEN was associated with several key molecules, including KRAS, Raf, MEK, ERK, PI3K, Akt, mTOR, Wnt, β-catenin, TGF-β and SMAD (Fig. 4A). To further confirm our prediction, by qRT-PCR assay we found that the RNA levels of PTEN were higher in 30 CRC tissues than in the paired normal tissues (P<0.0001, Fig. 4B). Furthermore, a correlation analysis was utilized to explore the correlation between LINC01559 and PTEN, revealing that LINC01559 expression is positively associated with PTEN in 30 pairs of CRC tissues (P =0.0031, Fig. 4C). Then, we used qRT-PCR to detect PTEN expression in a mouse model (Fig. 4D, P<0.01). We also analysed PTEN expression in different cell lines of CRC, including HCT116 (P<0.01), DLD-1 (P<0.01), and HT29 (P<0.01), which showed that downregulated LINC01559 could reduce PTEN expression at the RNA level (Fig. 4E). Moreover, PTEN

expression at the RNA level was observed at 36 h (P <0.05) and 48 h (P <0.01) in SW480 cells transfected with si-LINC01559-3 or the negative control vector. The results showed that the transfection efficiency of si-LINC01559 increased over time (Fig. 4F). Then, the results of IHC staining *in vivo* demonstrated that the protein expression of PTEN was significantly increased in the LA group (Fig. 3G). Thus, our results indicated that PTEN might be an anti-oncogene in CRC and could be regulated by LINC01559.

5. MiR-106b-5p is associated with LINC01559 in CRC

To investigate the mechanism of LINC01559 regulating PTEN, we analysed the potential miRNAs targeted by LINC01559 via DIANA tools - Tarbase v8, and 172 miRNAs were identified. Then, we characterized 118 miRNAs containing complementary sequences with PTEN via DIANA tools - LncBase Predicted v2. Through a Venn diagram, we selected a total of 10 shared miRNAs for further study (Fig. 5A, Additional file 3: Table S1). Then, by analysis of miRNA expression in CRC via a GEO dataset (GSE49246), we found that only hsa-miR-17-5p, hsa-miR-20a-5p, hsa-miR-20b-3p and hsa-miR-106b-5p were significantly increased in CRC tumor tissues, while the other miRNAs showed no significant differences. Then, we further analysed the difference in miRNA expression between CRC tissues and normal tissues through other GEO datasets, including GSE115513, GSE41655, GSE108153 and GSE110402. Furthermore, GSE56350 from the GEO database provided RNA expression results in tumor tissues in situ and metastatic tumor tissues. The results showed that miR-106b-5p and miR-17-5p were dramatically highly expressed in tumor tissues compared to normal tissues. Moreover, the expression of the two miRNAs was higher in metastatic tumor tissues than in tumor tissues in situ (Fig. 5B-G, Additional file 10: Figure S6). Based on these associative data and previous relevant studies, we explored the role of miR-106-5p in on the regulation of [30, 31]. Additionally, the qRT-PCR results showed that miR-106b-5p was commonly expressed at low levels in 30 paired CRC tissues. Confirming our previous findings, miR-106-5p was notably elevated in CRC tissues compared to normal tissues (Fig. 5H). Moreover, the expression of miR-106-5p was also increased with the downregulation of LINC01559 (Fig. 5I). Then, a FISH assay was utilized to examine LINC01559 distribution in the nucleus and cytoplasm. The results showed that LINC01559 was expressed both in the nucleus and cytoplasm and was more highly distributed in the cytoplasm (Fig. 5J).

To further determine whether miR-106b-5p could bind to the predicted target sites in LINC01559, we constructed three groups of LINC01559 luciferase reporter vectors: blank group (psiCHECK-2 vector), wild-type group (psiCHECK-2-LINC01559 WT) and mutant type group (the putative binding sites for miR-106b-5p were mutated, psiCHECK-2-LINC01559 MT). As expected, cotransfection of the wild-type LINC01559 vector (psiCHECK-2-LINC01559 WT) with miR-106b-5p mimics, but not the mutant LINC01559 vector (psiCHECK-2-LINC01559 MT), significantly reduced luciferase activities in HCT116 cells (P<0.01, Fig. 5K). We focused on the targets of miR-106b and found via a bioinformatics search in Starbase3.0 that the 3'-UTR of LINC01559 contained a region that matched the seed sequence of miR-106b-5p (Fig. 5L). To study the relationship between miR-106b-5p and PTEN, we constructed three groups of miR-106b-5p luciferase reporter vectors: blank group (psiCHECK-2 vector), wild-type group (psiCHECK-2-PTEN WT) and mutant type group (putative binding sites for PTEN were mutated, psiCHECK-2-PTEN MT). We found that

cotransfection of PTEN of the wild-type vector (psiCHECK-2-PTEN WT) with miR-106b-5p mimics, but not the mutant PTEN vector (psiCHECK-2–PTEN MT), significantly reduced luciferase activities in HCT116 cells (P<0.01, Fig. 5M). We also found that the 3′-UTR of PTEN contained a region that matched the seed sequence of miR-106b-5p (Fig. 5N). Finally, we analysed LINC01559 and miR-106b-5p expression in CRC tissues from different TNM-stage patients and paired normal tissues through ISH. ISH detected that LINC01559 expression in CRC tissues was lower than that in normal tissues, while miR-106b-5p expression was higher in CRC tissues (Fig. 5O). Altogether, our results indicated that LINC01559 might act as a molecular sponge for miR-106b-5p and that miR-106b-5p could regulate PTEN.

6. LINC01559 regulates the functions of CRC cells via miR-106b-5p to promote PTEN.

To clarify the relationship between LINC01559 and PTEN with respect to miR-106b-5p regulation, the HCT116 and SW480 cell lines were cotransfected with si-LINC01559 NC or si-LINC01559-3 and miR-106b-5p inhibitor NC or miR-106b-5p inhibitor. Then, the HCT116 and SW480 cell lines were divided into three groups: si-LINC01559 NC + miR-106b-5p inhibitor NC, si-LINC01559-3 + miR-106b-5p inhibitor NC and si-LINC01559-3 + miR-106b-5p inhibitor. qRT-PCR assays detected that LINC01559 knockdown compromised the suppressive regulation of PTEN by miR-106b-5p, as indicated by the reduced levels in both HCT116 and SW480 cells (Fig. 6A). By CCK-8 assays, we found that LINC01559 knockdown promoted CRC cell proliferation, while simultaneous miR-106b-5p knockdown completely reversed the promotion of cell proliferation in both SW480 and HCT116 cells (Fig. 6B). Similarly, miR-106b-5p knockdown also reversed the promotion of CRC cell migration, invasion and progression abilities using EdU assays and transwell assays (Fig. 6C, 6D). Downregulation of LINC01559 increased the protein expression of BCL-2 and N-cadherin but reduced the protein expression of E-cadherin in HCT116 cells, and this effect was countervailed by transfection with the miR-106b-5p inhibitor (Fig. 6E). Therefore, our results suggested that LINC01559 negatively regulated miR-106b-5p expression by interacting with PTEN (Fig. 6F).

7. METTL3 methylates LINC01559 to influence the function of CRC

Bioinformatics analysis by RMBase v2.0 demonstrated that LINC01559 contains 17 m6A modification sites, and m6A modification could influence LINC01559 regulation (Fig. 7A, Additional file 4: Table S2, Additional file 6: Figure S3). METTL3, as a key member of the m6A methyltransferase complex, has recently been reported to be highly expressed in metastatic CRC and associated with poor prognosis via diverse downstream genes [32]. Then, on account of the observed strong knockdown or amplification efficiency, we chose si-METTL3-1 as a representative siRNA for METTL3 and OV-METTL3 in SW480 cells by qPCR assays (Additional file 11: Figure S7). Using transwell assays and wound healing tests, we found that METTL3 knockdown inhibited CRC cell migration and invasion (Fig. 7B, 7C). To further explore whether the process of LINC01559 m6A methylation was influenced by METTL3, RIP-seq was performed, and the results indicated that METTL3 could bind to LINC01559 in SW480 cells (Fig. 7D). To explore whether METTL3 could modify LINC01559, cells with a stable increase in METTL3 were subjected to qRT-PCR. The results showed that overexpression of METTL3 inhibited the expression of LINC01559 in

SW480 cells ($P < 0.001$, Fig. 7E). Then, MERIP assays were used to explore the enrichment of m6A modification in LINC01559. Agarose gel electrophoresis (AGE) analysis following the MERIP assays was conducted to confirm the difference in RNA expression followed by immunoprecipitation with m6A antibody or IgG (control). The results revealed that the m6A modification in SW480 cells in the m6A group was approximately 32 times higher than that in the control group (normalized to the input, Fig. 7F). Accordingly, RIP assays and AGE were utilized to confirm the binding between LINC01559 and METTL3 in HCT116 and SW480 cell lines. The results showed that the complexes immunoprecipitated by the anti-METTL3 antibody contained overexpressed LINC01559 compared to the IgG group (normalized to the input, $P < 0.001$, Fig. 7G). To further confirm the function of METTL3 in CRC cells, MERIP assays were used to detect the methylation sites of LINC01559 in SW480 cells transfected with OV-METTL3. The results showed that, compared to those in the group transfected with OV-NC, m6A sites were upregulated by transfection with OV-METTL3 in SW480 cells (normalized to the input, $P < 0.001$, Fig. 7H).

To explore whether this activity, LINC01559 as a miR-106b-5p sponge, is mediated by METTL3, the HCT116 and SW480 cell lines were cotransfected with si-METTL3 NC or si-METTL3, and si-LINC01559 NC or si-LINC01559. Then, the HCT116 and SW480 cell lines were divided into three groups: si-METTL3 NC + si-LINC01559 NC, si-METTL3 + si-LINC01559 NC, and si-METTL3 + si-LINC01559. The results of qRT-PCR assays showed that downregulated METTL3 compromised the inhibition of miR-106b-5p by LINC01559 in HCT116 and SW480 cells(Fig. 7I). Meanwhile, there is no potential methylated sites of miR106b-5p though the bioinformatics prediction by SRAMP (Additional file 12: File S1).

Discussion

Previous studies showed that lncRNA expression was altered in a variety of human cancer types and that lncRNA expression patterns may be associated with metastasis and disease prognosis [33, 34]. Some reports also revealed that lncRNAs play an essential role in tumorigenesis and progression of tumors, and lncRNAs might be involved in transcriptional regulation either as cis- or trans-acting elements and could negatively or positively influence gene expression [35]. Furthermore, experiments *in vivo* also proved that the expression of specific lncRNAs with oncogenic or anti-oncogenic features is closely linked to the ability to influence matrix invasion of cancer cells and tumor growth [36]. Thus, research on the functions of lncRNAs in tumors is necessary to identify potential biomarkers in the prognosis and treatment of tumors. In our research, RNA-sequencing combined with qRT-PCR analysis revealed the downregulated expression pattern of LINC01559 in CRC tissues and cell lines, which was demonstrated to be associated with poor prognosis in CRC patients by clinical sample analysis. Our research highlighted the significant effects of LINC01559 during the complicated process of metastasis and proliferation through experiments *in vivo*. Consistent with our findings, it was also revealed that silencing LINC01559 restored the migratory, invasive and proliferative abilities and affected a number of key molecules, including PTEN. The results predicted that LINC01559 played an depressed role in CRC progression. Increasing evidence could also be found in previous study of rectal adenocarcinoma (READ) [37] and lung adenocarcinoma (LUAD) [38]. While, LINC01559 played a positive predictor in a lncRNA risk prognostic nomogram of hepatocellular carcinoma (HCC) [39]. Exosome-transferred LINC01559 from mesenchymal

stem cells (MSCs) could be transferred into gastric cancer (GC) cells to promote GC cell progression [40]. These pioneer studies implied that LINC01559 might develop the different functions in tumor specificity.

Recent studies proved that lncRNAs can affect diverse biological processes of cancers through the regulation of mRNA stability, RNA splicing, chromatin structure, and miRNA-mediated gene regulation by acting as miRNA sponges [41]. To our knowledge, high levels of lncRNAs are located in the cytoplasm, and cytoplasmic lncRNAs function as modulators by interacting with miRNAs, such as by acting as competitive endogenous RNAs (ceRNAs) [42]. It has been reported that the ceRNA network plays important roles in the occurrence and development of colorectal cancers, and most studies have demonstrated that lncRNAs and miRNAs are involved in ceRNA regulation [43]. CeRNA crosstalk depends on the miRNA response elements (MREs) located on each transcript, which together form the foundation of these coregulatory interactions [44]. In the present investigation, we demonstrated that miR-106b-5p could target MREs in LINC01559 through ceRNA interactions and could further influence the process of miR-106b-5p targeting PTEN.

We also explored the reason for the downregulated expression of LINC01559 in CRC cells. Recent studies revealed alterations in epigenetic regulation of ncRNAs via m6A methylation [45]. The distribution and functions of m6A in lncRNAs are poorly understood. Previous studies have found that m6A is detected in lncRNAs and that lncRNAs could be substrates for adenosine methylation [46]. It has been found that Olfr29-ps1 relies mainly on the m6A-modified Olfr29-ps1/miR-214-3p/MyD88 regulatory pathway to modulate myeloid-derived suppressor cell (MDSC) immunosuppression and differentiation [47]. Another study revealed that metastasis-associated lung adenocarcinoma transcript 1 (MALAT1) undergoes structural changes and localization due to m6A modifications and further regulates the interaction between RNAs and specific binding proteins [48]. In addition, it was revealed that altering the m6A modification level of lncRNA-1281 can significantly affect let-7 levels, thereby influencing ESC differentiation. However, research on how m6A works on lncRNAs in CRC is limited. In our research, we found potential m6A sites of LINC01559, and METTL3 could modify these sites to regulate the function of LINC01559 in CRC, which is also one of the highlights in our research.

Although our study did not explore the whole possible pathway of the effect of LINC01559 in CRC, our research, based on adequate evidence, revealed that LINC01559/miR-106b-5p/PTEN is a promising axis to suppress CRC progression. Furthermore, METTL3 could promote the m6A methylation level of LINC01559 transcripts to interfere with the suppressor role of LINC01559 in CRC.

Conclusions

In this research, we first uncovered that low LINC01559 expression could be an indicator of poor prognosis in patients with CRC. Furthermore, silencing LINC01559 significantly restored the proliferation ability of CRC cells. Research on the downstream molecular mechanism of LINC01559 demonstrated that the anti-oncogenic effect of LINC01559 is partly mediated through the inhibition of the activity of miR-106b-5p/PTEN. Notably, LINC01559 transcripts contain abundant m6A methylation sites, which provide

potential targets for METTL3. Our data highlighted an innovative m6A-dependent RNA regulatory mechanism in epigenetics and indicated a promising biomarker of CRC for improving individualized treatment for CRC patients (Fig. 8).

Abbreviations

miRNAs: microRNAs; mRNA: messenger RNA; 3'UTR: 3' untranslated region; EMT: epithelial-to-mesenchymal transition; qRT-PCR: quantitative reverse transcription polymerase chain reaction; CRC: colorectal cancer; TRN: trial registration number; OS: overall survival; WT: wild-type; READ: rectal adenocarcinoma; HCC: hepatocellular carcinoma; RCC: renal cell carcinoma; LUAD: lung adenocarcinoma; m6A: N6–methyladenosine; METTL3: methyltransferase-like 3; FISH: RNA fluorescence in-situ hybridization; RIP: RNA immunoprecipitation; RIP-seq: RNA immunoprecipitation sequencing; MeRIP: m6A RNA immunoprecipitation; H&E: haematoxylin-eosin; OV-METTL3: overexpressed METTL3 group; iCCAs: intrahepatic cholangiocarcinoma; MDSC: myeloid-derived suppressor cells; MALAT1: metastasis-associated lung adenocarcinoma transcript 1; NC: negative control; LN: anti-LINC01559 negative control group; LA: anti-LINC01559 group; WB: western blot analysis; MRE: miRNA response elements; AGE: agarose gel electrophoresis; mRNAs: messenger RNAs; MSCs: mesenchymal stem cells; GC: gastric cancer.

Declarations

Ethics approval and consent to participate

The human cancer tissues used in this study were approved by Ethnics Committee of The First Affiliated Hospital of Zhengzhou University in December 19, 2019, and the TRN is 2019-KW-423.

Consent for publication

All authors give consent for the publication of manuscript in ***Cell & Bioscience***.

Availability of data and materials

All the data obtained and/or analyzed during the current study were available from the corresponding authors on reasonable request.

Competing interests

The authors declare that they have no competing interests.

Funding

This study was supported by The National Natural Science Foundation of China (81972663, 81560385), Key Scientific Research Projects of Institutions of Higher Education in Henan Province (19A310024), The

Medical Scientific and Technological Research Project of Henan Province (201702027), The China Postdoctoral Science Foundation (2019T120648, 2017M610462), The National Natural Science Foundation of Henan Province (182300410342), The Health Commission Technology Talents Overseas Training Project of Henan Province (2018140) and The Key Scientific Research Project of Henan Higher Education Institutions (20A310024).

Authors' contributions

Conception and design: ZQS, JBL and WTY; Acquisition of data: KS, SXY, QBZ, CC, BS and YXG; Analysis and interpretation of data: LYZ, XXY and QGZ Writing, review, and/or revision of the manuscript: KS and SXY; Study supervision: GXW, ZQS, JBL and WTY. All authors read and approved the final manuscript.

Acknowledgements

Author details

[1]Department of Colorectal Surgery, The First Affiliated Hospital of Zhengzhou University, Zhengzhou 450052, Henan, China. [2]Academy of Medical Sciences, Zhengzhou University, Zhengzhou 450052, Henan, China. [3]School of Basic Medical Sciences, Zhengzhou University, Zhengzhou 450002, Henan, China. [4]Henan Academy of Medical and Pharmaceutical Sciences, Zhengzhou University, Zhengzhou 450052, Henan, China. [5]Department of Geriatric Medicine, The First Affiliated Hospital of Zhengzhou University, Zhengzhou 450052, Henan, China.

References

1. Bray F, Ferlay J, Soerjomataram I, et al: Global cancer statistics 2018: GLOBOCAN estimates of incidence and mortality worldwide for 36 cancers in 185 countries. CA: A Cancer Journal for Clinicians 2018, 68:394-424.

2. Huyghe JR, Bien SA, Harrison TA, et al: Discovery of common and rare genetic risk variants for colorectal cancer. Nature genetics 2019, 51:76-87.

3. Xu M, Chen X, Lin K, et al: The long noncoding RNA SNHG1 regulates colorectal cancer cell growth through interactions with EZH2 and miR-154-5p. Molecular cancer 2018, 17:141-141.

4. Bolha L, Ravnik-Glavač M, Glavač D: Long Noncoding RNAs as Biomarkers in Cancer. Disease Markers,2017,(2017-5-29) 2017, 2017:1-14.

5. Bhan A, Soleimani M, Mandal SS: Long Noncoding RNA and Cancer: A New Paradigm. Cancer Research 2017, 77:3965.

6. Kondo Y, Shinjo K, Katsushima K: Long non-coding RNAs as an epigenetic regulator in human cancers. Cancer Science 2017, 108:1927.

7. Hong JH, Jin EH: Correlations between Genetic Polymorphisms in Long Non-Coding RNA PRNCR1 and Gastric Cancer Risk in a Korean Population. 2019, 20.

8. Trapnell C, Hendrickson DG, Sauvageau M, et al: Differential analysis of gene regulation at transcript resolution with RNA-seq. Nat Biotechnol 2013, 31:46-53.

9. Cabili MN, Trapnell C, Goff L, et al: Integrative annotation of human large intergenic noncoding RNAs reveals global properties and specific subclasses. Genes Dev 2011, 25:1915-1927.

10. daSilva LF, Beckedorff FC, Ayupe AC, et al: Chromatin Landscape Distinguishes the Genomic Loci of Hundreds of Androgen-Receptor-Associated LincRNAs From the Loci of Non-associated LincRNAs. Frontiers in genetics 2018, 9:132-132.

11. Ponce-Castañeda MV, Lee M-H, Latres E, et al: p27Kip1: Chromosomal Mapping to 12p12–12p13.1 and Absence of Mutations in Human Tumors. Cancer Research 1995, 55:1211-1214.

12. Deng X, Su R, Weng H, et al: RNA N(6)-methyladenosine modification in cancers: current status and perspectives. Cell research 2018, 28:507-517.

13. Chen YG, Chen R, Ahmad S, et al: N6-Methyladenosine Modification Controls Circular RNA Immunity. Molecular cell 2019.

14. Chen B, Wang C, Zhang J, et al: New insights into long noncoding RNAs and pseudogenes in prognosis of renal cell carcinoma. Cancer cell international 2018, 18:157-157.

15. Yang D, Qiao J, Wang G, et al: N6-Methyladenosine modification of lincRNA 1281 is critically required for mESC differentiation potential. Nucleic acids research 2018, 46:3906-3920.

16. Bertero L, Massa F, Metovic J, et al: Eighth Edition of the UICC Classification of Malignant Tumours: an overview of the changes in the pathological TNM classification criteria-What has changed and why? Virchows Arch 2018, 472:519-531.

17. Kanehisa M, Araki M, Goto S, et al: KEGG for linking genomes to life and the environment. Nucleic Acids Research 2008, 36:D480-D484.

18. Kanehisa M, Goto S, Sato Y, et al: KEGG for integration and interpretation of large-scale molecular data sets. Nucleic Acids Research 2012, 40:D109-D114.

19. Tang Z, Li C, Kang B, et al: GEPIA: a web server for cancer and normal gene expression profiling and interactive analyses. Nucleic Acids Research 2017, 45.

20. Karagkouni D, Paraskevopoulou MD, Chatzopoulos S, et al: DIANA-TarBase v8: a decade-long collection of experimentally supported miRNAâ“gene interactions. Nucleic Acids Research 2018, 46:D239-D245.

21. Hulsen T, Vlieg JD, Alkema W: BioVenn – a web application for the comparison and visualization of biological lists using area-proportional Venn diagrams. Bmc Genomics 2008, 9:488.

22. Yang W, Li Y, Song X, et al: Genome-wide analysis of long noncoding RNA and mRNA co-expression profile in intrahepatic cholangiocarcinoma tissue by RNA sequencing. Oncotarget 2017, 8:26591-26599.

23. Jun-Hao L, Shun L, Hui Z, et al: starBase v2.0: decoding miRNA-ceRNA, miRNA-ncRNA and protein-RNA interaction networks from large-scale CLIP-Seq data. Nucleic Acids Research 2014, 42:D92.

24. Zhou Y, Zeng P, Li YH, et al: SRAMP: prediction of mammalian N6-methyladenosine (m6A) sites based on sequence-derived features. Nucleic Acids Res 2016, 44:e91.

25. Georgouli M, Herraiz C, Crosas-Molist E, et al: Regional Activation of Myosin II in Cancer Cells Drives Tumor Progression via a Secretory Cross-Talk with the Immune Microenvironment. Cell 2019, 176:757-+.

26. Chen R-X, Chen X, Xia L-P, et al: N6-methyladenosine modification of circNSUN2 facilitates cytoplasmic export and stabilizes HMGA2 to promote colorectal liver metastasis. In Nature communications, vol. 10. pp. 46952019:4695.

27. Shen L, Qu X, Li H, et al: NDRG2 facilitates colorectal cancer differentiation through the regulation of Skp2-p21/p27 axis. Oncogene 2018, 37:1759-1774.

28. Kim RH, Mak TW: Tumours and tremors: how PTEN regulation underlies both. British journal of cancer 2006, 94:620-624.

29. Laurent-Puig P, Cayre A, Manceau G, et al: Analysis of PTEN, BRAF, and EGFR Status in Determining Benefit From Cetuximab Therapy in Wild-Type KRAS Metastatic Colon Cancer. Journal of Clinical Oncology 2009, 27:5924-5930.

30. Li N, Miao Y, Shan Y, et al: MiR-106b and miR-93 regulate cell progression by suppression of PTEN via PI3K/Akt pathway in breast cancer. Cell Death & Disease 2017, 8:e2796.

31. Zheng L, Zhang Y, Liu Y, et al: MiR-106b induces cell radioresistance via the PTEN/PI3K/AKT pathways and p21 in colorectal cancer. Journal of translational medicine 2015, 13:252-252.

32. Li T, Hu PS, Zuo Z, et al: METTL3 facilitates tumor progression via an m6A-IGF2BP2-dependent mechanism in colorectal carcinoma. Molecular Cancer 2019, 18:112.

33. Yang X, Xie X, Xiao Y-F, et al: The emergence of long non-coding RNAs in the tumorigenesis of hepatocellular carcinoma. Cancer Letters, 360:119-124.

34. Chen F, Tian Y, Pang E-j, et al: MALAT2-activated long noncoding RNA indicates a biomarker of poor prognosis in gastric cancer. Cancer Gene Therapy.

35. Liz J, Esteller M: lncRNAs and microRNAs with a role in cancer development. Biochimica et Biophysica Acta (BBA) - Gene Regulatory Mechanisms 2016, 1859:169-176.

36. Qiu MT, Hu J-W, Yin R, et al: Long noncoding RNA: an emerging paradigm of cancer research. Tumour Biology the Journal of the International Society for Oncodevelopmental Biology & Medicine, 34:613-620.

37. Zhu X, Wang D, Lin Q, et al: Screening key lncRNAs for human rectal adenocarcinoma based on lncRNA-mRNA functional synergistic network. Cancer medicine 2019, 8:3875-3891.

38. Shi X, Tan H, Le X, et al: An expression signature model to predict lung adenocarcinoma-specific survival. Cancer management and research 2018, 10:3717-3732.

39. Zhang Z, Ouyang Y, Huang Y, et al: Comprehensive bioinformatics analysis reveals potential lncRNA biomarkers for overall survival in patients with hepatocellular carcinoma: an on-line individual risk calculator based on TCGA cohort. Cancer cell international 2019, 19:174-174.

40. Wang L, Bo X, Yi X, et al: Exosome-transferred LINC01559 promotes the progression of gastric cancer via PI3K/AKT signaling pathway. Cell death & disease 2020, 11:723-723.

41. Kondo Y, Shinjo K, Katsushima K: Long non-coding RNAs as an epigenetic regulator in human cancers. Cancer Sci 2017, 108:1927-1933.

42. Ulitsky I, Bartel DP: lincRNAs: genomics, evolution, and mechanisms. Cell 2013, 154:26-46.

43. Shuwen H, Qing Z, Yan Z, et al: Competitive endogenous RNA in colorectal cancer: A systematic review. Gene 2018, 645:157-162.

44. Tay Y, Rinn J, Pandolfi PP: The multilayered complexity of ceRNA crosstalk and competition. Nature 2014, 505:344-352.

45. Fu Y, Dominissini D, Rechavi G, et al: Gene expression regulation mediated through reversible m(6)A RNA methylation. Nat Rev Genet 2014, 15:293-306.

46. Meyer KD, Saletore Y, Zumbo P, et al: Comprehensive analysis of mRNA methylation reveals enrichment in 3' UTRs and near stop codons. Cell 2012, 149:1635-1646.

47. Shang W, Gao Y, Tang Z, et al: The Pseudogene Olfr29-ps1 Promotes the Suppressive Function and Differentiation of Monocytic MDSCs. Cancer Immunology Research 2019, 7:813-827.

48. Zhou KI, Parisien M, Dai Q, et al: N(6)-Methyladenosine Modification in a Long Noncoding RNA Hairpin Predisposes Its Conformation to Protein Binding. Journal of molecular biology 2016, 428:822-833.

Figures

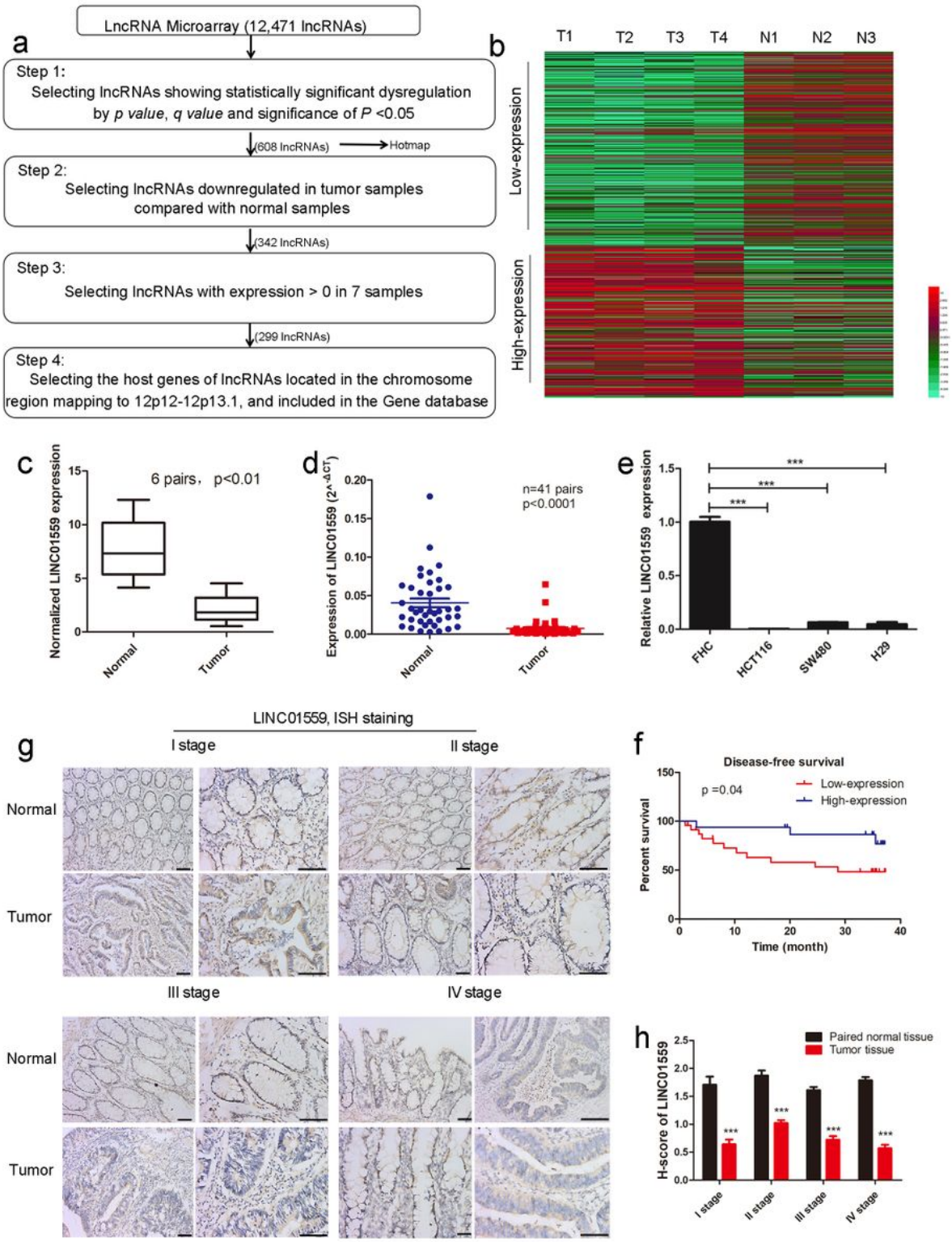

Figure 1

LINC01559 is expressed at low levels in CRC, and the downregulation of LINC01559 is associated with poor prognosis. (a) Flowchart illustrating the screening criteria of potential regulatory lncRNAs enriched in CRCs (p value<0.05, q value<0.05; T1, T2, T3 and T4 indicate tumor samples; N1, N2 and N3 indicate normal intestinal mucosa samples). (b) Clustered heatmap showing the dysregulated expression of lncRNAs after the selection at step 4. (c) LINC01559 expression by high-throughput sequencing of 6 paired CRC tumor tissues (Tumor) and adjacent normal tissues (Normal). (d) qRT-PCR analysis of LINC01559 expression in CRC tissues from patients (T, n=30) and paired normal tissues (N, n=30). (e) qRT-PCR analysis of LINC01559 expression in CRC cell lines (HCT116, SW480 and H29) compared to the normal intestinal mucosa cell line (FHC). (f) Kaplan-Meier plots of disease-free survival according to different LINC01559 expression groups (P=0.04). (g) and (h) ISH staining for LINC01559 expression levels in CRC tissues and H-score for ISH staining at different TNM stages of CRC (Scale bar = 100 μm, scale bar = 50 μm; I stage n=1, II stage n=2, III stage n=3, IV stage n=2; three images were obtained for each sample). The data in (b), (c), (d), (e) and (f) were analysed by Student's t-test and are presented as the mean ± SD. (*P < 0.05, **P < 0.01, ***P < 0.001)

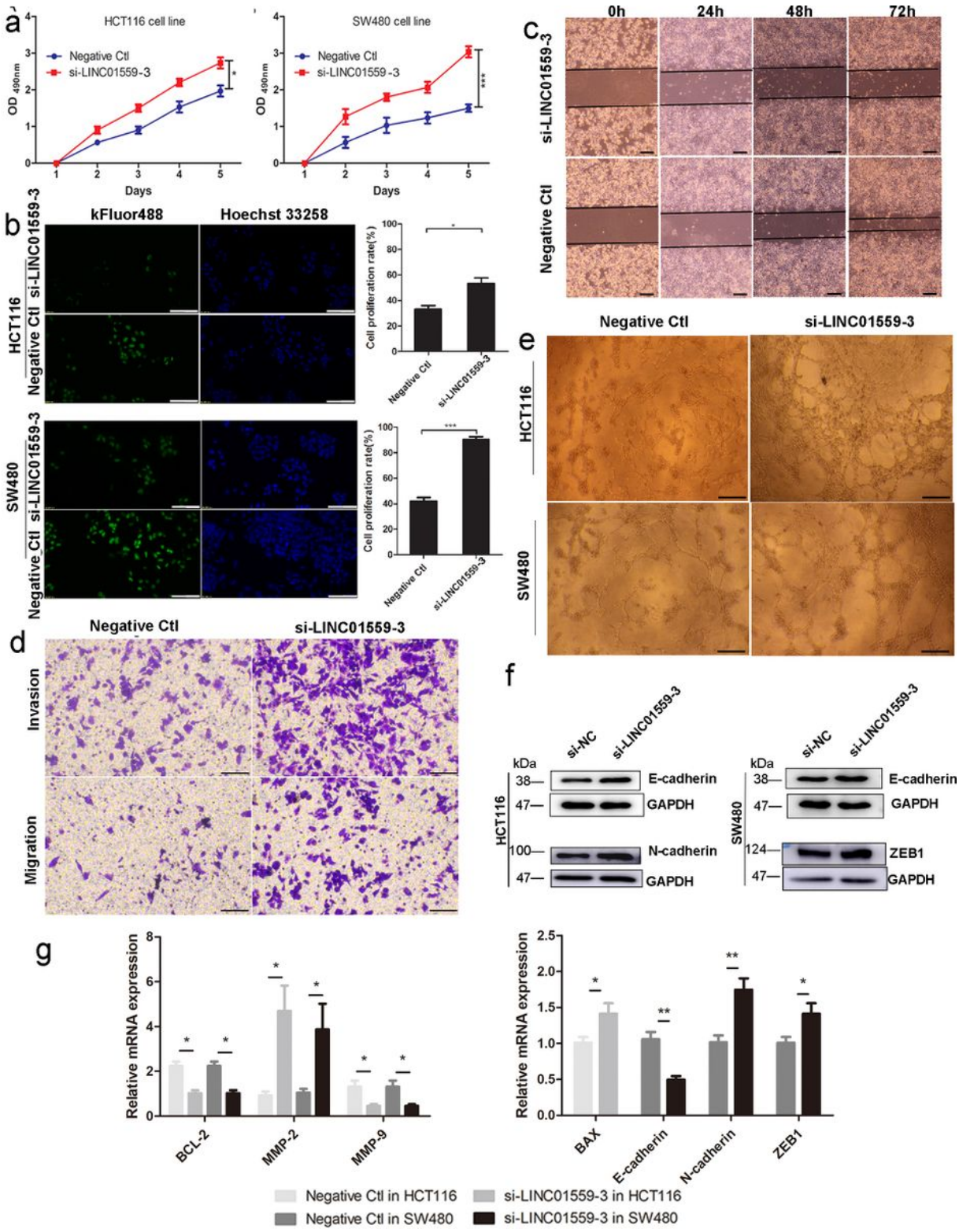

Figure 2

Downregulated LINC01559 enhances CRC cell proliferation and metastasis in vitro. HCT116 and SW480 cell lines were transfected with si-LINC01559-3 or the negative control vector (Negative Ctl). Cell proliferation was determined with a CCK-8 assay (a) and EdU staining (scale bar = 50 μm) (b). Cell metastasis was detected through a wound healing assay (scale bar = 100 μm) (c) and a transwell assay (scale bar = 50 μm) (d). Representative images of the tube formation assay show the vascularization

capacity of CRC cells (e). Results of differential gene expression with WB (f) and qRT-PCR (normalized to GAPDH) (g). The data in (a), (b) and (g) were analysed by Student's t-test and are presented as the mean ± SD. (*P < 0.05, **P < 0.01, ***P < 0.001)

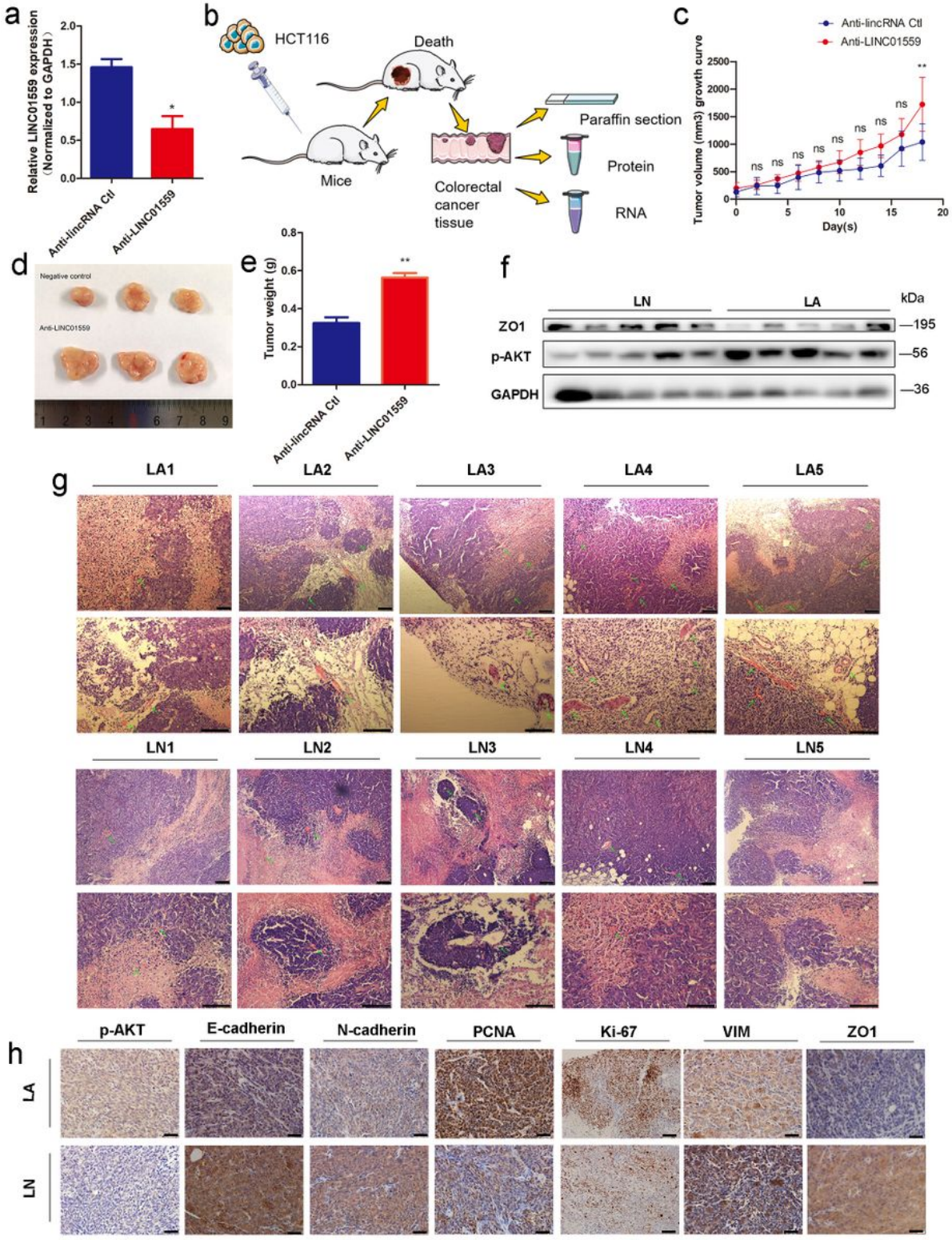

Figure 3

Downregulated LINC01559 enhances CRC progression in vivo. HCT116 cells were transfected with anti-LINC01559 or anti-LINC01559 control vector and then injected into nude mice. The subcutaneous tumor

models were divided into two groups: anti-LINC01559 negative control group (LN) and anti-LINC01559 group (LA) (n = 5 mice per group). qRT-PCR was used to examine the expression of LINC01559 to estimate the transfection efficiency (normalized to GAPDH) (a). Schematic depiction showing the construction process of the CRC subcutaneous tumor model (b). The tumor volume growth curves (c), tumor size (d) and tumor weight (e) after implantation in different groups. WB analysis of ZO1 and p-AKT protein expression in LA compared to LN (f). Representative images showing blood vessel distribution and density of tumor samples from different groups by H&E staining (scale bar =200 μm and 100 μm) (g). Representative images showing the protein expression of PTEN, p-AKT, E-cadherin, N-cadherin, PCNA, Ki-67, VIM and ZO1 from different tumor groups (scale bar = 100 μm) (h). The data in (A) and (C) were analysed by Student's t-test and are presented as the mean±SD. (*P < 0.05, **P < 0.01, ***P < 0.001, ns: no significance)

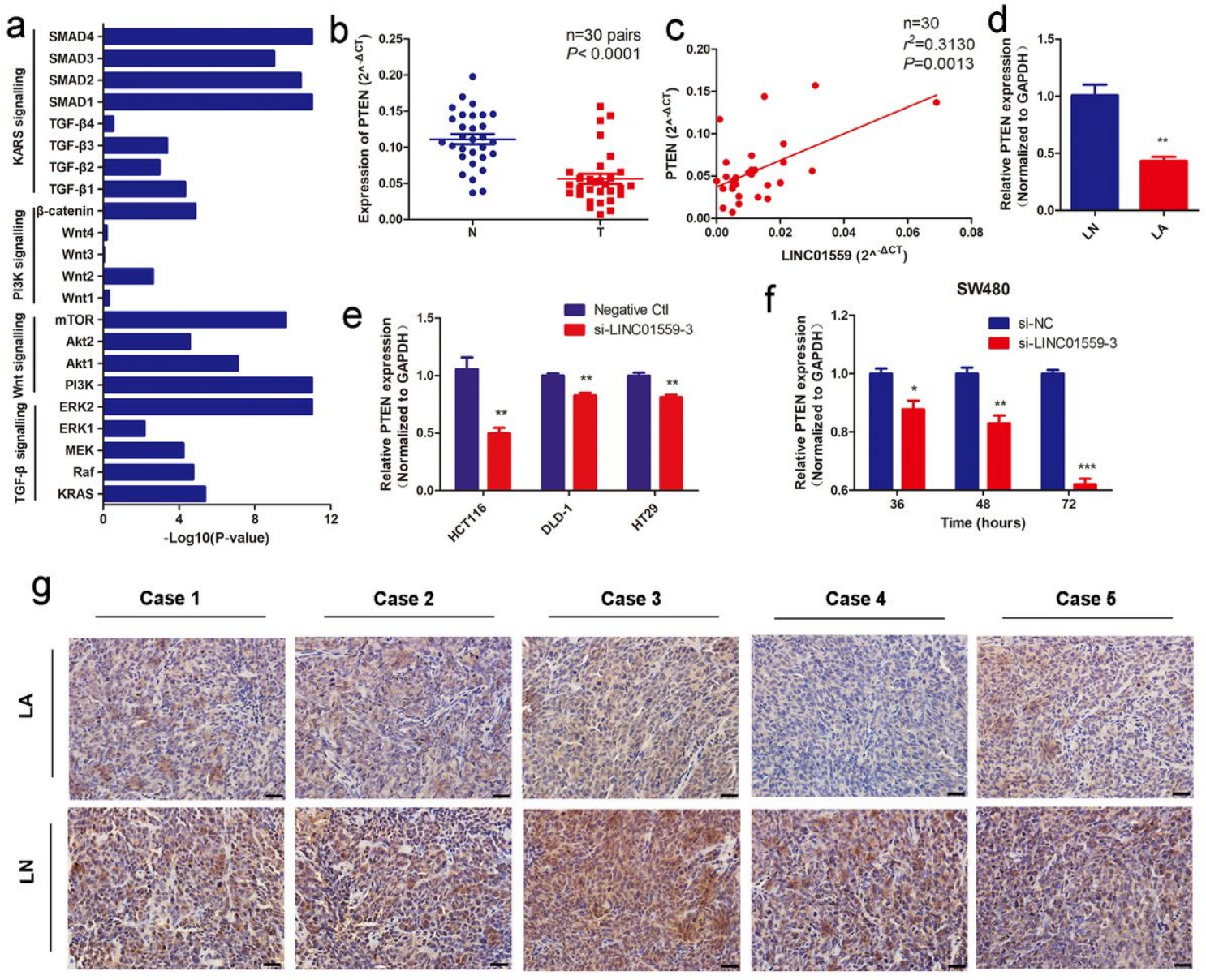

Figure 4

PTEN is associated with LINC01559 and is expressed at low levels in CRC. (a) The correlation between PTEN and key molecules in signalling pathways of CRC. (b) PTEN expression was detected by qRT-PCR in 30 pairs of colorectal cancer tissues (T) compared to adjacent normal tissues (N) (n =30, P <0.0001). (c) The correlation between PTEN mRNA expression and LINC01559 expression analysed in 30 pairs of colorectal cancer samples (n=30, r2=0.31, P =0.0013) (normalized to GAPDH). (d) PTEN expression was detected by qRT-PCR in different tumor groups of subcutaneous tumor models (n = 5) (normalized to GAPDH). (e) PTEN expression was detected by qRT-PCR in different cell lines transfected with si-LINC01559-3 or the negative control vector (Negative Ctl) (normalized to GAPDH). (f) qRT-PCR was used to explore PTEN expression in SW480 cells after 36 or 48 hours of transfection with si-LINC01559-3 or the negative control vector (Negative Ctl) (normalized to GAPDH). (g) Representative images showing the protein expression of PTEN in five mice bearing tumors from different groups (scale bar =100 μm). The data in (a), (b), (c), (d), (e) and (f) were analysed by Student's t-test and are presented as the mean ± SD. (*P < 0.05, **P < 0.01, ***P < 0.001)

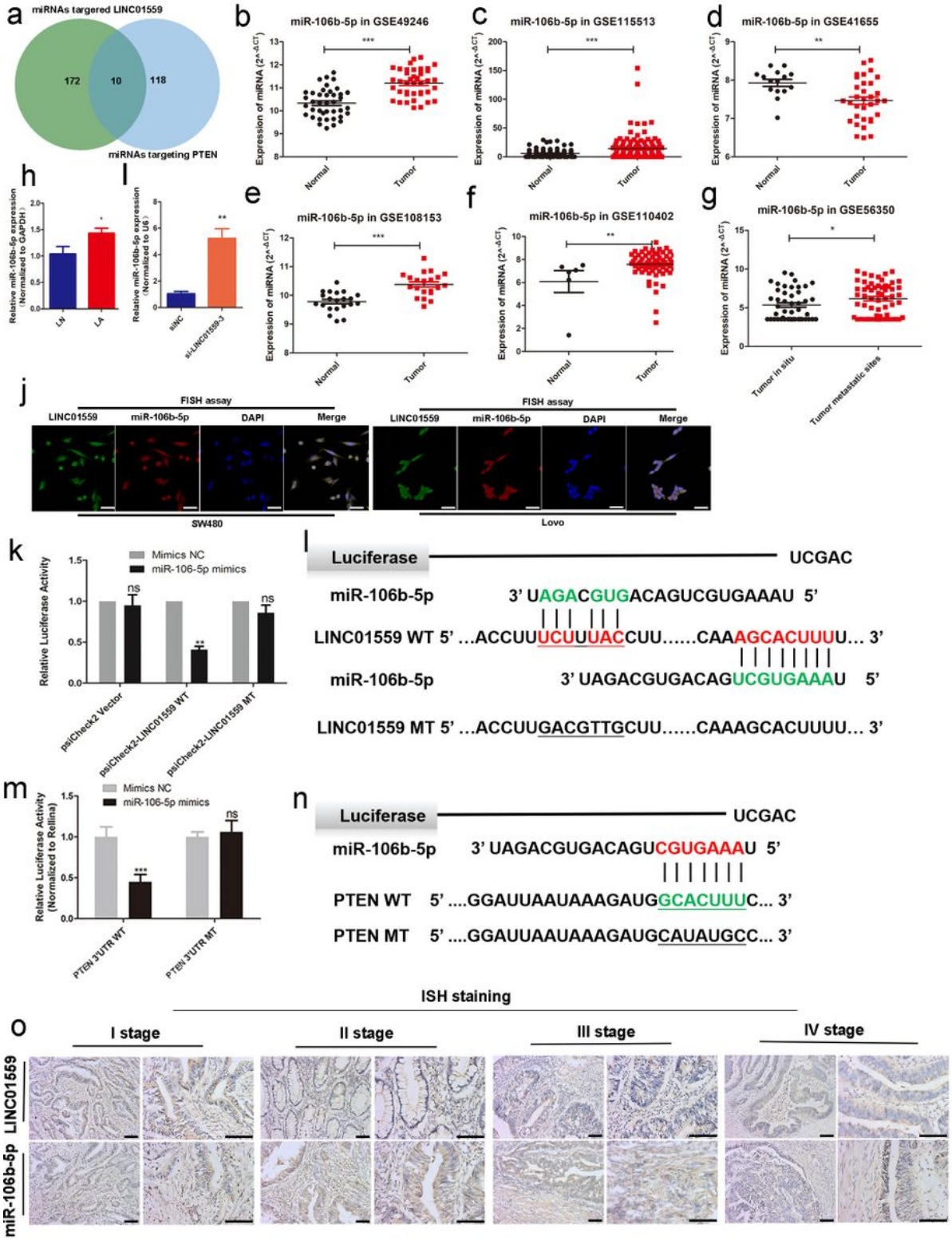

Figure 5

miR-106b-5p is associated with LINC01559 in CRC. (a) Venn diagram showing the shared miRNAs between miRNAs targeting LINC01559 and miRNAs targeting PTEN. (b-g) MiR-106b-5p expression was analysed in the GEO datasets GSE49246, GSE115513, GSE41655, GSE108153, GSE110402 and GSE56350. (h) MiR-106b-5p expression was detected by qRT-PCR in different groups of subcutaneous tumor models in nude mice (n=5). (i) MiR-106b-5p expression was measured by qRT-PCR in HCT116 cells

transfected with si-LINC01559-3 or the negative control vector (Negative Ctl). (j) FISH assays were carried out to determine the nuclear-cytoplasmic fractionation of LINC01559 and miR-10b-5p in SW480 and lovo cells (green: LINC01559, red: miR-106b-5p, blue: DAPI, purple: merge, scale bar =50 μm). (k) A luciferase reporter assay was performed to detect the interaction between LINC01559 and miR-106b-5p. (l) The binding site sequences on LINC01559 for miR-106b-5p were obtained from Starbase3.0 and were mutated to the complementary sequences. (m) A luciferase reporter assay was performed to detect the interaction between miR-106b-5p and PTEN (scale bar =50 μm). (n) The biding site sequences on miR-106b-5p for PTEN were obtained from Starbase3.0 and were mutated to the complementary sequences. (o) ISH staining for LINC01559 or miR-106b-5p expression levels in CRC tissues at different TNM stages of CRC (scale bar =100 μm or 50 μm; I stage n=1, II stage n=2, III stage n=3, IV stage n=2; three images were obtained for each sample). In the schematic diagram of l and n, green and red indicate interacting sequences, and underscore indicates wild type and matched mutant sequences. The data in (b), (c), (d), (f), (g), (h), (k) and (m) were analysed by Student's t-test and are presented as the mean ± SD. (*P < 0.05, **P < 0.01, ***P < 0.001)

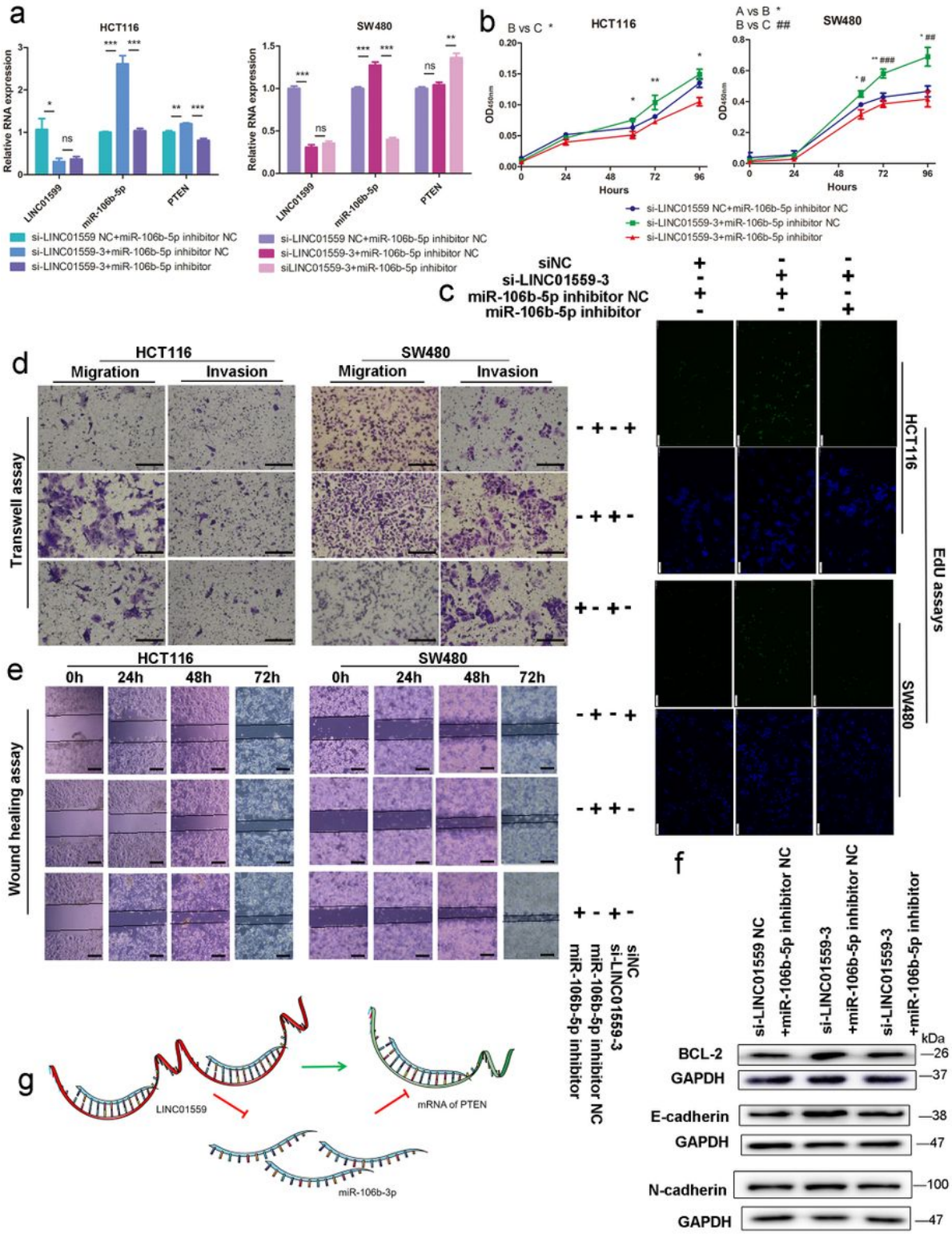

Figure 6

LINC01559 regulates the functions of CRC cells via miR-106b-5p to promote PTEN. HCT116 and SW480 cells were cotransfected with an siRNA against LINC01559 and a miR-106b-5p inhibitor. qRT-PCR was used to examine the expression of LINC01559, miR-106b-5p and PTEN after cotransfection (miR-106b-5p: Normalized to U6, LINC01559 and PTEN: Normalized to GAPDH) (a). Cell proliferation was determined with a CCK-8 assay (b) and EdU staining (scale bar =100 μm) (c). Cell migration and invasion were

detected by transwell assays (scale bar =50 μm) (d). The results of the WB test showed the protein expression levels of different genes (e). Schematic representation of a model depicting that LINC01559 negatively regulated miR-106b-5p expression by interacting with PTEN (f). In Figure 6b, A, black: si-LINC01559 NC + miR-106b-5p inhibitor NC, B, green: si-LINC01559 + miR-106b-5p inhibitor NC, and C, red: si-LINC01559 + miR-106b-5p inhibitor. The data in (a) and (b) were analysed by Student's t-test and are presented as the mean ± SD. (Scale bar: 50 μm, */# P < 0.05, **/##P < 0.01, ***/###P < 0.001, ns: no significance)

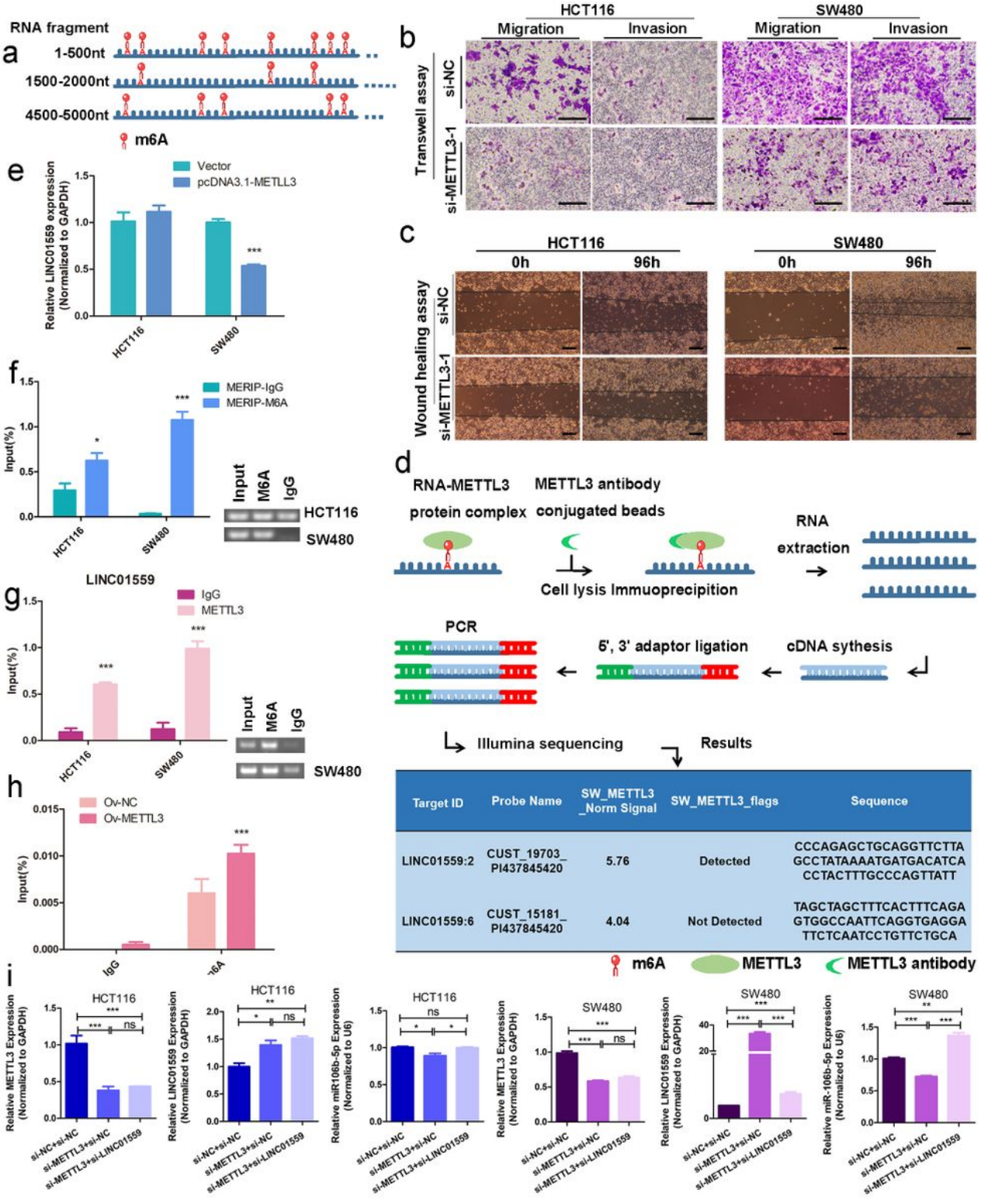

Figure 7

METTL3 methylates LINC01559 to influence the function of CRC. (a) Schematic representation of a model depicting m6A modification peaks in LINC01559. Wound healing assays (scale bar =100 μm) (b) and transwell assays (scale bar =50 μm) (c) were utilized to prove the role of METTL3 in CRC. (d) The flow map of the RIP-seq process analysed by METTL3 protein antibody showed the possibility of METTL3 binding to LINC01559. (e) LINC01559 expression was detected by qRT-PCR in HCT116 and SW480 cells transfected with METTL3 overexpression vector (pcDNA3.1-METTL3) or negative control vector (vector). (f) MERIP assays and AGE assays were used to explore the enrichment of m6A modification in LINC01559. The percentage of the input in the SW480 group is shown. (g) RIP assays and AGE assays confirmed the binding between LINC01559 and METTL3 in HCT116 and SW480 cell lines. (h) MERIP assays detected the methylation sites of LINC01559 in SW480 cells transfected with OV-METTL3. (i) Q-PCR assays was used to examine the expression of METTL3, LINC01559, and miR-106b-5p after cotransfection (miR-106b-5p: Normalized to U6, METTL3 and LINC01559: Normalized to GAPDH). The data in (e), (f), (g), (h) and (i) were analyzed by Student's t-test and are presented as the mean ± SD. (*P < 0.05, **P < 0.01, ***P < 0.001, ns: no significance)

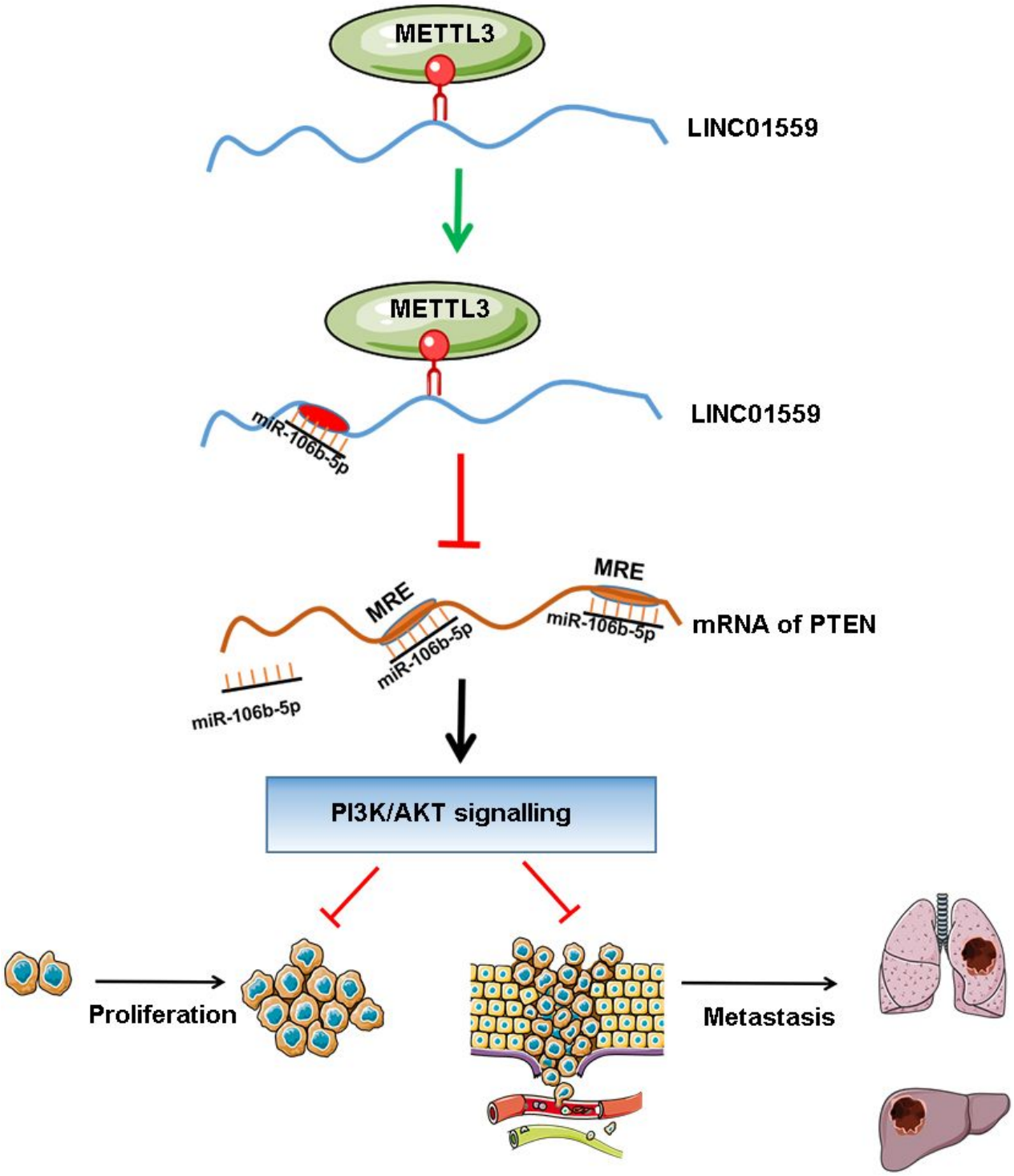

Figure 8

Schematic representation of a model depicting the major molecular mechanisms of the LINC01559/miR106b-5p/PTEN axis in CRC.

Supplementary Files

This is a list of supplementary files associated with this preprint. Click to download.

- Additionalfile12FileS1.pdf
- Additionalfile3TableS1.xlsx
- Additionalfile4TableS2.xlsx
- SupplementalInformation.doc